Available online at www.sciencedirect.com
SCIENCE DIRECT®
Earth and Planetary Science Letters 241 (2006) 387–397
EPSL
www.elsevier.com/locate/epsl

The thermal structure of subduction zones constrained by seismic imaging: Implications for slab dehydration and wedge flow

Geoffrey A. Abers [a,*], Peter E. van Keken [b,1], Erik A. Kneller [b], Aaron Ferris [a], Joshua C. Stachnik [c]

[a] Department of Earth Sciences, 685 Commonwealth Ave., Boston University, Boston, MA 02215, USA
[b] Department of Geological Sciences, 1100 North University Ave., University of Michigan, Ann Arbor, MI 48109-1005, USA
[c] Alaska Earthquake Information Center, Geophysical Institute, University of Alaska, Fairbanks, AK 99775, USA

Received 7 April 2005; received in revised form 28 November 2005; accepted 28 November 2005
Available online 6 January 2006
Editor: R.D. van der Hilst

Abstract

Thermal models of subduction zones often base their slab–wedge geometry from seismicity at mantle depths and, consequently, cannot be used to evaluate the relationship between seismicity and structure. Here, high-resolution seismic observations from the recent Broadband Experiment Across the Alaska Range (BEAAR) constrain, in a rare instance, the subducting slab geometry and mantle wedge temperature independent of seismicity. Receiver functions reveal that the subducting crust descends less steeply than the Wadati-Benioff Zone. Attenuation tomography of the mantle wedge reveals a high Q and presumably cold region where the slab is less than 80 km deep. To understand these two observations, we generate thermal models that use the improved wedge geometry from receiver functions and that incorporate temperature- and strain-rate-dependent olivine rheology. These calculations show that seismicity within the subducting crust falls in a narrow belt of pressure–temperature conditions, illuminating an effective Clapeyron slope of 0.1 K/MPa at temperatures of 450–750 °C. These conditions typify the breakdown of high-pressure hydrous minerals such as lawsonite and suggest that a single set of dehydration reactions may trigger intermediate-depth seismicity. The models also require that the upper, cold nose of the mantle wedge be isolated from the main flow in the mantle wedge in order to sustain the cold temperatures inferred from the Q tomography. Possibly, sufficient mechanical decoupling occurs at the top of the downgoing slab along a localized shear zone to 80 km depth, considerably deeper than inferred from thrust zone seismicity.

Keywords: subduction; thermal models; Alaska; receiver functions; intermediate-depth earthquakes; mantle wedge

1. Introduction

Forward modeling of the thermal structure of subduction zones provides important insights into the conditions for generation of arc volcanism and generation of earthquakes. Commonly, studies prescribe the geometry and motion of the subducting slab and assume that this drives convection dynamically in the overlying mantle wedge, which in turn lies below an immobile

* Corresponding author. Tel.: +1 617 353 2616; fax: +1 617 353 3290.
E-mail addresses: abers@bu.edu (G.A. Abers), keken@umich.edu (P.E. van Keken), ekneller@umich.edu (E.A. Kneller), aferris@bu.edu (A. Ferris), josh@giseis.alaska.edu (J.C. Stachnik).
[1] Tel.: +1 734 764 1497.

0012-821X/$ - see front matter © 2005 Elsevier B.V. All rights reserved.
doi:10.1016/j.epsl.2005.11.055

lithospheric plate. In most cases, the interface between slab and wedge is inferred from the Wadati-Benioff Zone (WBZ) geometry, allowing estimation of thermal structure in variety of subduction zones (e.g., [1]). However, the lack of control of the top of the downgoing plate independent of seismicity makes it difficult to rigorously test theories of how intermediate-depth seismicity is generated. WBZ earthquakes likely result from thermal and mineralogical changes within, rather than on top of, the downgoing plate [2]. More generally, the lack of high-resolution constraints on proxies for temperature in the mantle wedge and slab allow for a wide range of thermal models to be consistent with observations [3,4].

Recently, it has become possible to image the top of the subducting plate to great depths, independently from seismicity, using mode-converted phases either from earthquakes within the downgoing plate [5] or from teleseismic P to S converted phases that are often analyzed as receiver functions [6–8]. At the same time, advances in dynamical modeling and our understanding of mantle materials have made it possible to consider more realistic thermal models that incorporate non-Newtonian temperature-dependent rheology, hydrolytic weakening and the effects of buoyancy (e.g., [3,9,10]).

In this paper, we will use new observational constraints to construct improved models of the central Alaskan subduction zone (Fig. 1). In particular, seismic measurements constrain the position of the subducting crust from receiver functions in relation to intermediate-depth earthquakes [8] and the broad thermal structure of the mantle wedge from attenuation tomography [11]. These results can be used to constrain and evaluate candidate thermal models. For a range of reasonable parameters, we infer seismicity to lie upon a linear path in pressure–temperature space rather than an isotherm, which strongly suggests that a mineral reaction front controls the position of the earthquakes in the subducting slab.

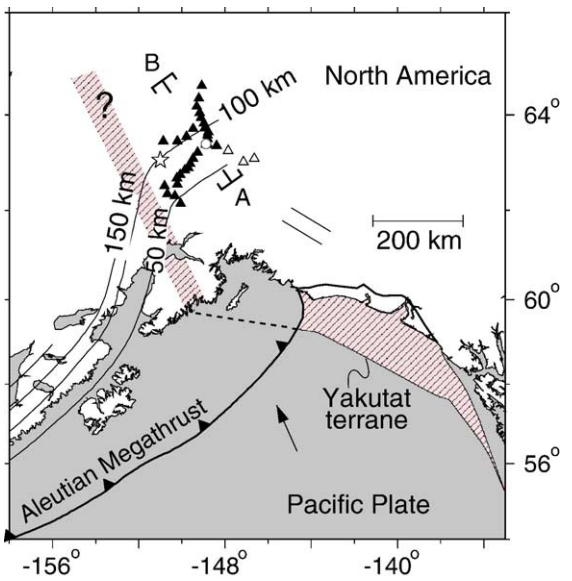

Fig. 1. The central Alaska subduction zone and BEAAR stations (triangles), after [8]. Brackets labeled A–B show location of transect in subsequent figures; open circle shows center of coordinates used in plots. Barbed line shows Aleutian trench and contours, labeled, show depth to Wadati-Benioff Zone. Dashed line shows presumed westward extension of Yakutat terrane from magnetic anomalies [52].

2. Observations

2.1. Downgoing plate from receiver functions

Teleseismic receiver functions from the Broadband Experiment Across the Alaska Range (BEAAR; Fig. 1) reveal a thick low-velocity layer (LVL) at the top of the downgoing plate from 60 to 120 km depth [8]. This LVL is hypothesized to be crust of the subducting Yakutat terrane, an accreted oceanic plateau or tectonically thickened oceanic crust (Fig. 2). As depth increases, the LVL exhibits a gradual increase in seismic velocity consistent with progressive dehydration and eclogitization. The LVL becomes indistinct from the surrounding mantle at 125–140 km depth, which coincides with the depth range over which WBZ seismicity stops. These earthquakes all lie within the LVL and traverse its entire thickness. The WBZ dips slightly steeper than does the LVL, descending into the subducting crust in a manner reminiscent of a reaction front. In most other slabs, the subducting crust is only 6 km thick, which makes it much more difficult to see the relationship between subducted crust and seismicity, with few exceptions [7,12].

Error analysis [8] suggests that random errors in depth to LVL and WBZ seismicity are both on the order 2–4 km, consistent with the small scatter in both datasets about smooth surfaces (Fig. 2). Systematic errors have been minimized by using only stations within or close to the BEAAR array to locate earthquakes, so that both the hypocenters and slab surface are constrained by similar ray paths passing through similar-velocity material. (Note that a small plotting error in [8] has been corrected on Fig. 2, resulting in the same slab geometry but conversion points relocated farther up the dip of the slab.) We improve the results of [8] by relocating earthquakes and the LVL in a preliminary three-dimensional (3D) velocity model [13]. The

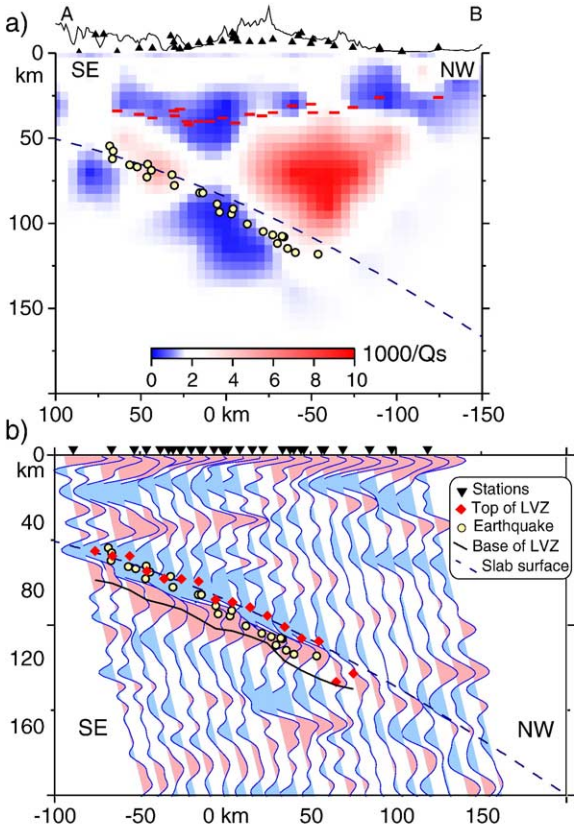

Fig. 2. Cross-sections showing results from BEAAR, along cross-section A–B in Fig. 1. (a) Attenuation (1/Qs) tomography [11]. Red lines: crustal thickness from receiver functions [13]; yellow circles: relocated earthquakes; dashed line: polynomial fit to slab surface. Top shows topography and projected station locations, triangles, with 10× vertical exaggeration. (b) Receiver function results, modified from [8]. Traces show interpolated receiver function wavefield, back-projected in one-dimensional velocity model to P–S conversion points. Red diamonds: top of slab LVZ from waveform inversion; solid line: base of LVZ; yellow circles: earthquakes; dashed line: fit slab surface. The LVZ and hypocenters differ from [8], in that both are determined in a three-dimensional velocity model so more accurately incorporate velocity gradients within the wedge. A minor plotting error was also corrected.

velocity inversion uses an identical ray distribution for P and S, to minimize the effects of resolution differences on the ratio of P to S velocities (Vp/Vs) [14]. The resulting velocities exhibit a decrease in Vp/Vs toward the northwest in the mantle wedge, from roughly 1.80 to 1.70. Receiver functions are inverted for LVL parameters in a velocity structure approximating the 3D model, by vertically averaging crust and wedge velocities beneath each station. The resulting LVL differs by less than 1 km from that published previously [8], but hypocenters move up by 5 to 10 km depending on depth (Fig. 3). The WBZ dips more steeply than the LVL in both velocity models, such that deeper earthquakes lie farther from the top of the slab.

To further test the extent of systematic bias in these locations, we relocate both the LVL and WBZ locations of Ferris et al. [8] in a suite of 16 end-member one-dimensional velocity models (Fig. 3). In each test, P-wave velocity (Vp) and the Vp/Vs ratio for the crust and mantle are perturbed to the limits of values allowed by travel-time observations: Vp ranges over 6.5–6.8 km/s and 7.7–8.0 km/s, and Vp/Vs over 1.75–1.85 and 1.65–1.75, for crust and mantle, respectively. The bounds constitute maximal limits allowed by regional differential travel times and by receiver function multi-

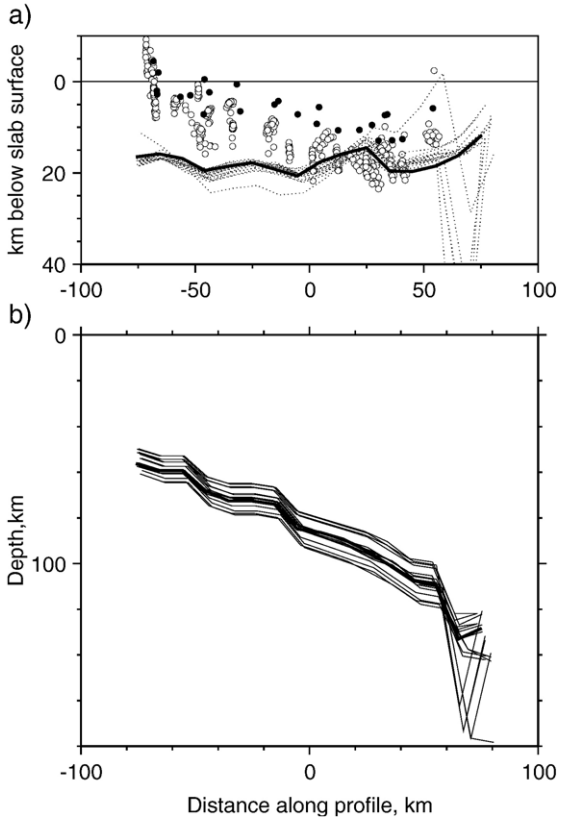

Fig. 3. Sensitivity of earthquake locations and slab surface depth to assumed seismic velocity model. Both earthquakes and top of slab are located in 16 one-dimensional velocity models, spanning the plausible range of Vp and Vp/Vs for crust and mantle. (a) Location of earthquakes, circles, and base of LVZ, dashed line, as distance below top of slab. Solid circles and thick lines show comparable result for three-dimensional velocity model used in Fig. 2. (b) Top of the slab, determined by inversion in the manner of [8] for all 16 models. In all cases, earthquakes descend from top to bottom of the low velocity layer as the subducting plate descends from 50–60 km to 90–110 km. Thus, the observation of earthquakes progressively getting deeper in the slab is robust.

ples [11,13]. The location of the top of LVL (Fig. 3a) varies by 10–15 km between tests, but in all cases the earthquakes progressively descend from the top to bottom of the LVL with increasing depth (Fig. 3b). At the deepest parts of the LVL, the slab depth shows higher sensitivity to the assumed velocities, but here the relevant signals are weak and the LVL velocity anomalies are small. Overall, the relative location of the WBZ relative to the LVL is a robust feature of these data and earthquakes clearly descend into the downgoing plate with increasing depth.

2.2. Attenuation and thermal structure

Much of the overlying mantle wedge exhibits high seismic attenuation (low Q; Fig. 2) [11]. At the high pressures expected in the mantle, porosity should be very low and attenuation should be dominated by thermally activated processes [15,16], although small amounts of melt and water could have an important secondary effect [17,18]. Seismic attenuation is relatively unaffected by composition. Hence, to first order, regions of low Q should correspond to high temperatures. The overlying mantle wedge shows high Q, indicating low temperatures, where the slab is less than 80 km deep, but low Q farther into the wedge. This "cold nose" is expected to be a relatively rigid part of the upper mantle and indicates relative isolation from wedge flow. It provides a region cold enough for ultramafic hydrous phases such as serpentine and chlorite, which hold large concentrations of water [19] to be stable. A similar "viscous nose" has been observed on the basis of low attenuation in Japan [20] and the central Andes [21], and is likely a common feature of subduction zones. Heat flow data are available for only a few subduction zones and generally show a pattern of low heat flow between the trench and a region 10–30 km seaward of the volcanic arc. This coincides with the location below which high Q is observed [22–25]. Thermal models confirm that low heat flow can only be matched with the presence of such a cold region [3,26].

3. Thermal models

To explain these observations we have developed a number of steady-state models for the central Alaska subduction zone (Fig. 4). The model setup including the governing equations and solution methods closely follows [3], but is calibrated to the slab geometry and other parameters for Alaska. The slab surface below the BEAAR array is constrained to intersect the trench at the Earth's surface and to roughly follow the major velocity discontinuities thought to represent the active thrust fault offshore [27]. At depths greater than 60 km, the surface follows the top of the LVL (dashed line on Fig. 2).

Flow in the mantle wedge is computed by solving the equations of conservation of mass and momentum for a viscous medium. The base of the mantle wedge is prescribed to move with the slab, while the top of the wedge is in rigid contact with the overriding plate. The side boundary is a stress-free inflow/outflow boundary. With these conditions, the velocity in the wedge is determined only by the drag of the slab at the base and the viscosity of the wedge, which in turn depends on temperature and strain rate. The heat advection–diffusion equation is solved for the entire domain assuming a rigid overriding plate and a prescribed descent rate for the slab that is parallel to the top of the slab. We take the depth of the rigid portion of the overriding lithosphere to be 50 km.

For our base model, we use a convergence speed of $V=55$ mm/yr based on the Nuvel-1A plate model [28] and an age of the oceanic lithosphere of 38 Ma at the trench [29]. We do not have strong constraints on the effective shear heating along the seismogenic zone due to the paucity of heat flow measurements in this region. Based on the low estimates for effective shear rate in other subduction zones [3,26], we will use a effective shear stress of $\tau=10$ MPa along the seismogenic zone in our base model, which corresponds to a shear heating of $\tau V=17$ mW/m^2. We will display temperature fields only in the 'region of interest' defined in Fig. 4. Calculations use a finite element method to solve the governing equations following [3]. The model grid has approximately 70,000 linear elements and 35,000 nodal points. The grid resolution in the corner flow region, where the strongest boundary layers occur, is slightly less than 1 km on average (Fig. 4b).

Fig. 5a shows the temperature structure (left panel) for the model assuming an isoviscous rheology in the mantle wedge and with flow allowed up to the end of the seismogenic zone at 50 km depth. The phase diagram (right panel) predicts the pressure (p) and temperature (T) conditions at the earthquakes. These are compared to the temperature at the top of the slab and at the bottom of the thickened oceanic crust (black lines) and the lawsonite–dehydration curves suggested by field relations [30], experiments [31] and thermodynamic calculations [32]. Lawsonite, a Ca–Al-rich silicate with 11 wt.% H_2O, is probably the main phase holding H_2O at pressures above 2.5 GPa in mafic rock [33], although at lower pressures a sequence of hydrous phases continuously breaks down in subducting crust to

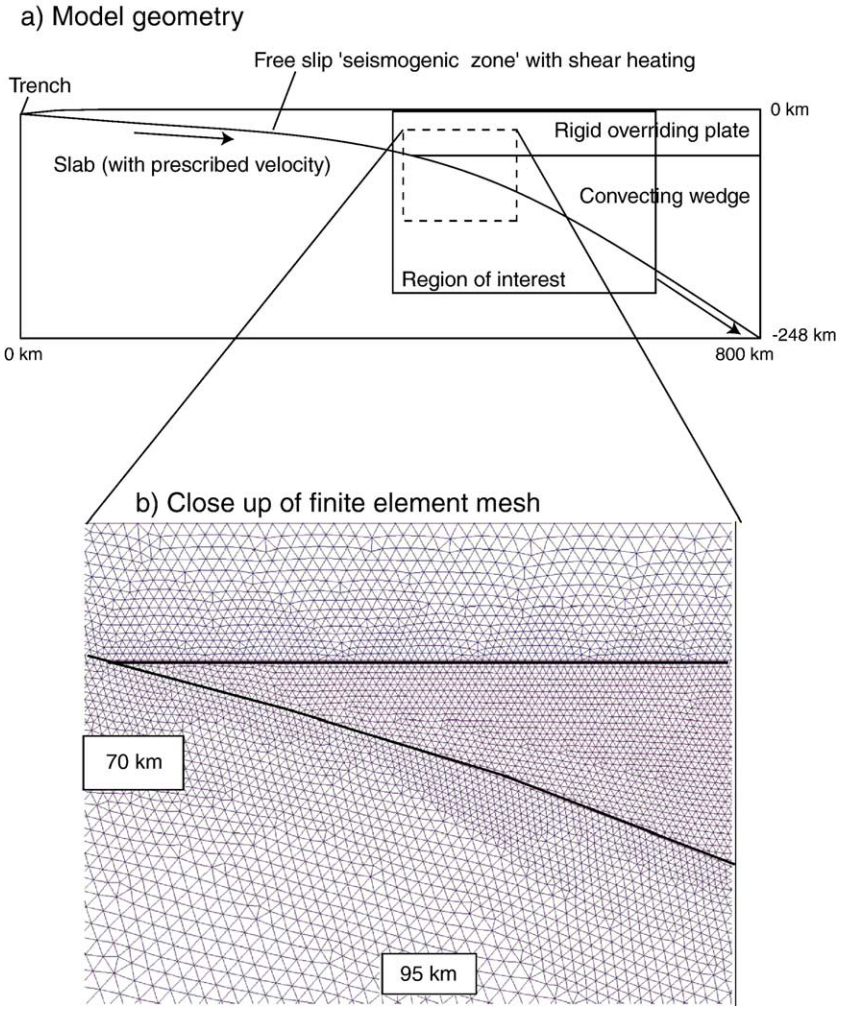

Fig. 4. (a) Model geometry. The slab velocity is kinematically described with a velocity parallel to the slab surface. The overriding plate is modeled as a rigid body. The mantle wedge is driven by the subducting plate and the velocity is computed from the governing Stokes equations [3]; (b) close up of computational mesh showing linear triangles. The average resolution near the corner point is less than 1 km.

release fluid into the wedge [31,32]. The earthquakes follow a (p,T) path that is intermediate between the predictions [30–32]. The temperature at the earthquake hypocenters increases with pressure at a rate of approximately 0.1 K/MPa but with a fair amount of scatter at shallow pressures.

It is more realistic to model the mantle of the wedge as a medium with strongly temperature- and stress-dependent rheology, which is characteristic of the deformation of the dominant minerals under mantle conditions. In Fig. 5b, we show the temperature field obtained with rheology based on dislocation creep in dry olivine [34]. Compared with isoviscous results, the temperature-dependence causes a focusing of the flow toward the nose of the wedge and the temperature along the slab-wedge increases strongly (also see [3,4]). The temperature at the base of the thickened crust is relatively unaffected. The use of the more realistic rheology causes a dramatic change in the predicted temperature of the earthquakes at $p<2.5$ GPa, which shift well above any of the experimentally determined dehydration curves and enhances the scatter at $p<3$ GPa.

One significant failure this model (Fig. 5b) is the prediction of high temperatures and hence high seismic attenuation throughout the mantle wedge below 50 km depth, in conflict with observations (Fig. 2). Similar behavior has been observed in several recent models incorporating variable-viscosity mantle [3,4,35]. By contrast, the Q tomography indicates relatively cool conditions in the nose of the wedge with a near-vertical boundary between the high Q (low T) and low Q (high

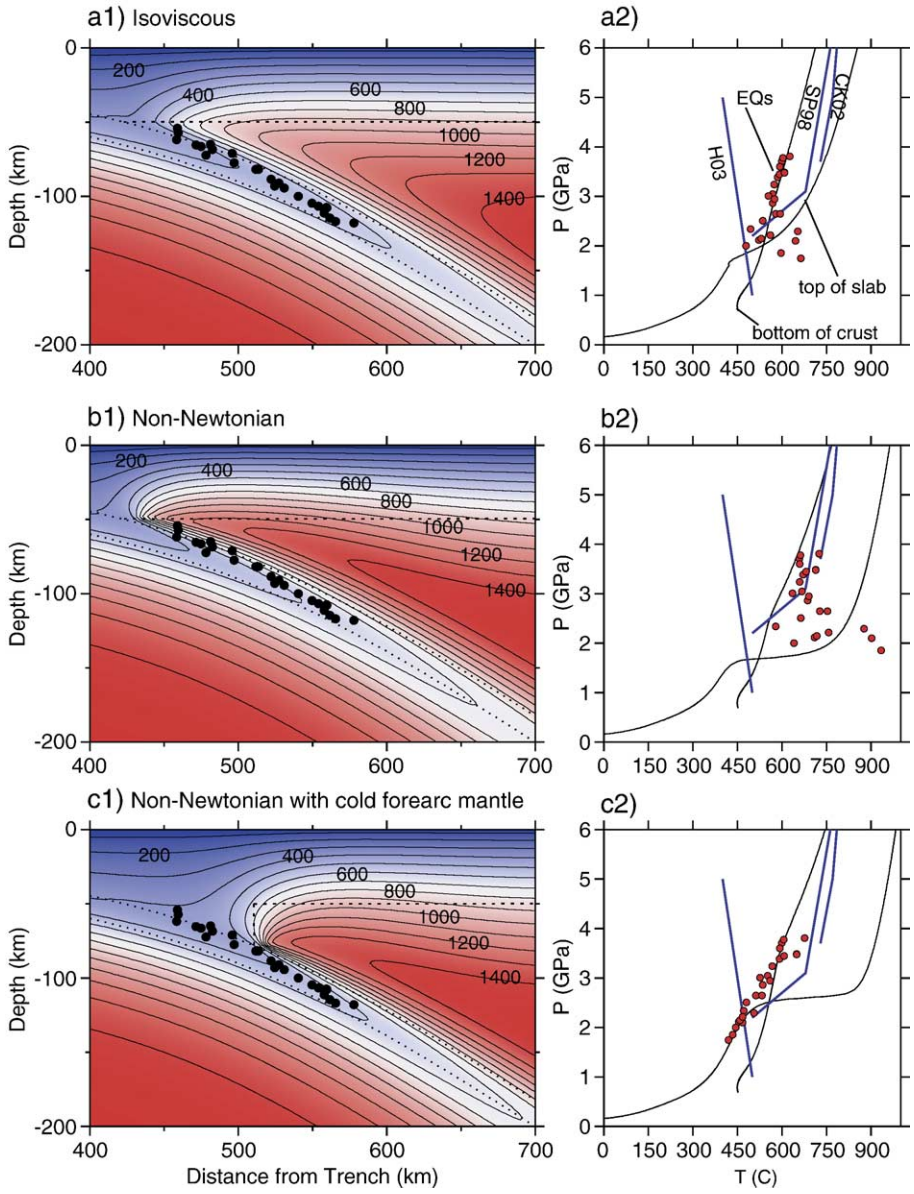

Fig. 5. Base model results for (a) isoviscous rheology, (b) non-Newtonian temperature-dependent rheology (based on creep law for dry olivine), (c) as in (b) but with a non-convecting portion of the mantle wedge (the 'cold nose') above 80 km depth. Left column displays the temperature field with a contour interval is 100 °C. Right column shows the (p, T) relationship at the top and bottom of the thickened crust (black lines) and the earthquakes (red circles) after addition of a constant 0.3 K/km adiabatic gradient. Blue lines indicate petrological constraints on the lawsonite-out boundary based on field relations (H03) [30], from experiments (SP98) [31] and from thermodynamic calculations (CK02) [32]. EQs: earthquakes.

T). We simulate this pattern by adding a vertical boundary in the tip of the mantle wedge where the slab surface is at 80 km depth (see stippled line in Fig. 5c) and we do not allow flow through this boundary, following previous work [3,26]. The slab surface is now exposed to the high temperature mantle wedge at greater pressure and the earthquakes follow a coherent (p,T) path. While the addition of this vertical boundary is ad hoc, it does better resemble the attenuation observations. Thus, some process to decouple the cold nose from the mantle wedge flow appears needed to explain the Q observations.

It is instructive to investigate the sensitivity of the model to variations in the main input parameters. Fig. 6 shows the (p,T) conditions predicted in the earthquake locations for variations in age of the lithosphere at the trench (from 30 to 50 Myr; Fig. 6a), subduction speed V (from 45 to 65 mm/yr; Fig. 6b) and the amount of shear

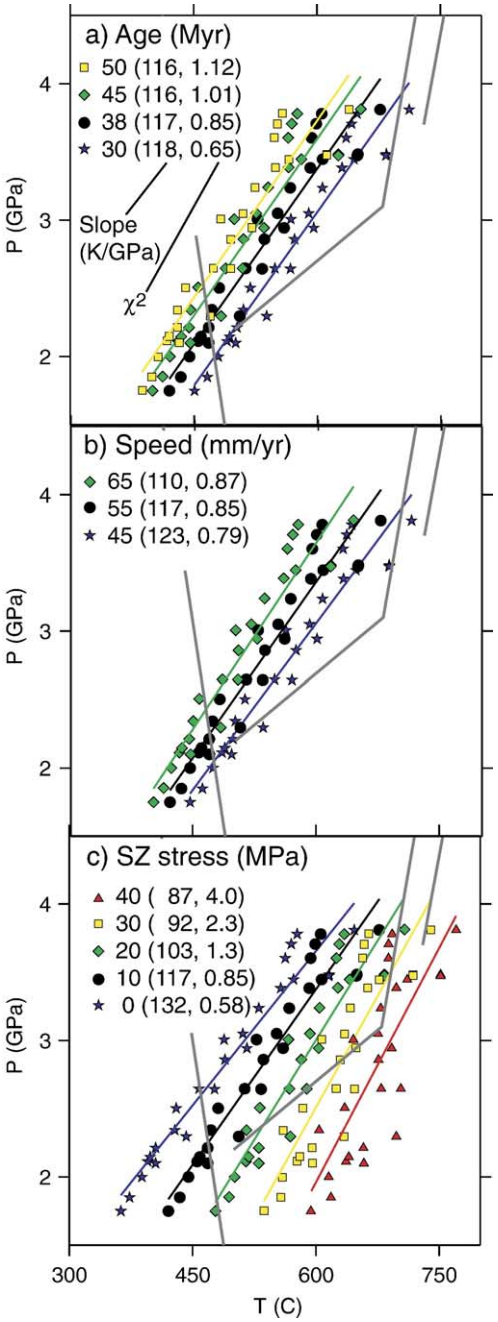

Fig. 6. Sensitivity of earthquake (p, T) conditions as a function of (a) plate age, (b) plate speed and (c) assumed shear stress along the seismogenic zone.

heating along the seismogenic zone (following stress that varies from 0 to 40 MPa; Fig. 6c). The black circles represent the (p,T) conditions in the earthquakes in our preferred model. The straight lines represent the least-squares fit to the earthquake (p,T) conditions. We indicate both the slope of the line and χ^2, which gets smaller as the quality of the fit gets better. The (inverse) slope of the best fit line in our preferred model is 117 K/GPa. The slope or quality of fit do not vary significantly for variations in speed or age, but the earthquake (p,T) conditions are systematically offset to higher temperature for decreases in both age and speed. Variations in shear heating have their largest effect at shallow depths and consequently the slope decreases with increasing shear stress. The predicted earthquake (p,T) conditions also tend to be less coherent for shear stress values larger than 20 MPa due to significant spread at lower pressures. These relationships hold for hypocenters located in the tomographic model as well as in the one-dimensional model.

4. Discussion

4.1. Dehydration and seismogenesis

The deepest earthquakes along this section lie near 120 km depth, close to the point at which seismic velocities within the LVZ become indistinct from surroundings. The coincidence of the depth cutoff with velocities supports the notion that dehydration processes in the downgoing plate are in some way triggering seismicity here and that (in Alaska) dehydration is confined to the subducting crust [8]. In other subduction zones, the LVZ and WBZ are harder to distinguish, because low-velocity layers are of a few km thickness. In general, an LVZ has been observed at depths that seismicity is present but not deeper [2,36]. In Alaska the WBZ earthquakes gradually descend from the top to bottom of the LVZ, as the slab surface descends from 60 to 120 km depth, a result that appears robust and well within uncertainties (Fig. 3). As a consequence, they lie within a narrow band of (p,T) conditions (Figs. 5 and 6). The narrow (p,T) range of the earthquakes suggests that a simple reaction front is responsible for the triggering of the earthquakes. The effective Clapeyron slope of 0.1 K/MPa is a robust feature of all our models except in the case of high shear heating along the fault. Shear heating is not directly constrained in Alaska, but based on other subduction zones with reliable heat flow data the effective shear stress is probably 10 MPa or less [37]. The events do not occur at isothermal conditions, as would be expected for models of seismogenesis appealing to runaway thermally activated creep. Thus, we infer that phase changes, likely involving dehydration, control the nucleation of earthquakes.

The linearity of seismicity in (p,T) is intriguing. Dehydration reactions in metabasalts occur nearly con-

tinuously over a wide range of depths [31,38], which would predict earthquakes throughout the thickness of the hydrated layer. In Alaska, such a seismic zone should be 15–20 km thick zone where the slab is shallow, but this would be much thicker than observed. One possible explanation is that dehydration reactions are more univariant than predicted in the laboratory, at least for the lithologies subducting here. Alternatively, the dehydration reactions at pressures below 2.5 GPa for some reason cannot trigger earthquakes, but they can be triggered by a subsequent, major univariant reaction associated with large H_2O release and volume change. The main dehydration reaction at 2.5–6 GPa within mafic rocks is the breakdown of lawsonite [33], which should occur at roughly the conditions at which WBZ seismicity is seen. There is some uncertainty in the actual location of this reaction boundary; field relations indicate lawsonite breaks down in mafic rocks at <500 °C [30], while experiments [31] and thermodynamic calculations [32] indicate that lawsonite is stable up to 600–700 °C. The dehydration reaction appears to be complex and continuous below the lawsonite-boundary [31], potentially complicating the distribution of available H_2O. Also, kinetic effects may delay the reaction [39]. Given these uncertainties, the seismicity could be associated with lawsonite breakdown, or along some other similar univariant reaction (for example, serpentine in ultramafic rocks breaks down at similar temperatures [30]). It therefore is possible that a simple dehydration reaction may be controlling seismicity, as suggested by the linearity of seismicity in (p,T).

Even if such reactions occur, other conditions for seismogenesis could be absent except at certain points of the dehydration path. Simple models of dehydration embrittlement [40] produce earthquakes by elevating pore pressure upon dehydration, so that only reactions with sufficiently positive Clapeyron slopes will generate positive pressure changes. The rate of reaction-driven pressure increase must exceed the rate of fluid escape, so slight volume increases may not generate earthquakes depending upon permeability. While the final lawsonite-out reaction shows a positive Clapeyron slope at 3–8 GPa [31,38], many earlier reactions may not, and a gradual breakdown of hydrous phases might not proceed rapidly enough to outpace intergranular fluid flow. The structure and evolution of permeability within the downgoing plate is almost completely unknown, and its influence on seismogenesis is difficult to quantify. Finally, recent experiments [41] indicate that serpentine dehydration can lead to fault formation even at a negative Clapeyron slope, indicating a more complex relationship may exist between dehydration and unstable slip.

4.2. Deep interplate slip and the cold nose

The interplate seismogenic zone extends 30–50 km deep in most subduction zones [42]. To mimic this behavior, subduction-zone thermal models often impose some form of mechanical decoupling to a depth of 50 km [1,4]. Such an assumption clearly oversimplifies the actual rheology at the plate interface down-dip of the thrust zone, where there is likely to be an extended transition between localized, frictionally unstable sliding and completely distributed flow. Immediately down-dip of the seismogenic zone, a region should exist which is conditionally stable with respect to friction, in which earthquakes cannot nucleate but rupture of large earthquakes can propagate seismically [43]. The recent observation of transient creep events, at time scales of days to months (e.g., 44,45]) suggests that localized slip occurs down-dip of the seismogenic zone in an episodic manner. Steady localized creep has been inferred down-dip of thrust zones in south–central Alaska from geodetic observations [46]. While the contribution to total slip from such phenomena is not yet well constrained, their existence implies a region of highly localized deformation not well described by the wedge rheology used here. Finally, studies of exhumed faults show that localized ductile shear occurs through a range of processes at increasing pressure and temperature, by a variety of plastic processes (e.g., 47]). Hence, some form of localized shear probably occur down-dip of subduction zone thrusts, potentially aided by the likely presence of frictionally weak phases such as serpentine and talc in hydrated peridotites.

Such a shear zone provides an explanation for the observation of a frequent “cold nose” seen in seismic attenuation data [11,21,48], which indicates some mechanical decoupling of the shallow mantle wedge. The cold nose is difficult to reproduce without special boundary conditions that either force the flow down along the vertical boundary (as in Fig. 5c) or simulate a weak shear zone atop the slab. Separate work [49] has suggested that a gradual coupling of the slab to the overlying wedge can accurately reproduce the apparent temperature structure. Another suggestion comes from Conder [50] who shows that the use of a parameterization of the brittle–ductile transition can also lead to deeper decoupling and reproduce similar distributions for temperature. In Fig. 7, we show the effects of partial decoupling between the slab and the wedge on the

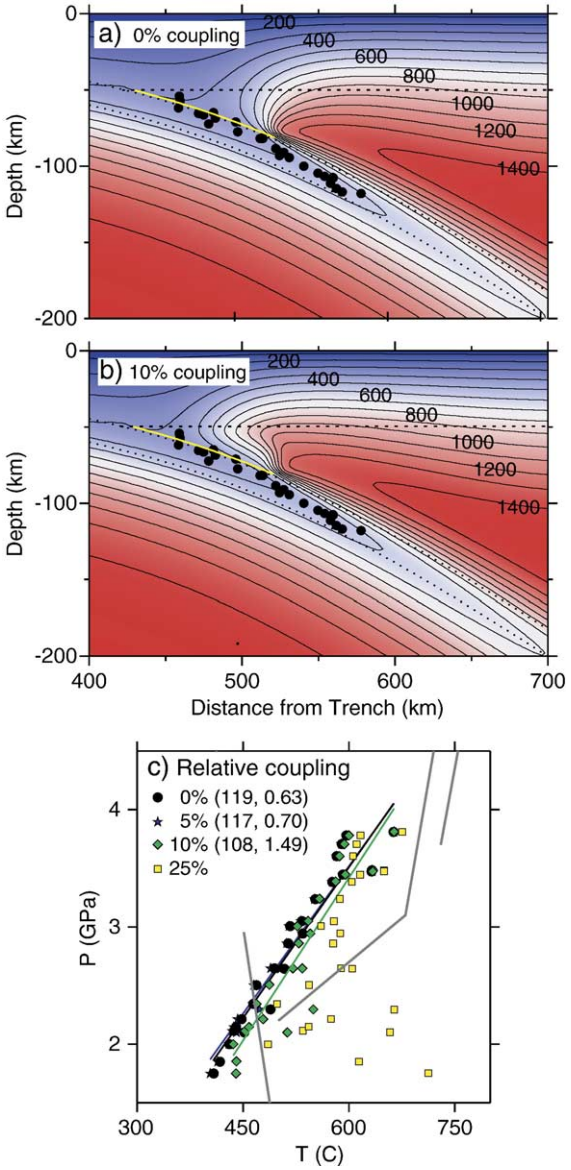

Fig. 7. Models illustrating the effect of partial decoupling between the slab and wedge below the seismogenic zone. (a) Model where the velocity at the base of the wedge is 0% of that of the slab in the depth range of 50–80 km. (b) Same for a velocity reduction of 10%. (c) Sensitivity of the predicted (p, T) conditions.

Alaska subduction zone model. In this case, we reduce the velocity prescribed at the base of the slab to 0–25% of the velocity of the subducting slab in the region where the slab surface is between 50 and 80 km deep, while allowing flow into the wedge corner. This slip geometry resembles that inferred from inversion of geodetic measurements, which also indicate localized slip to 70–80 km depth beneath Alaska [51]. A strong vertical division occurs in these thermal models for coupling up to 10%, similar to that seen in the Q tomography, between hot and cold regions. We conclude that the cold wedge nose may be generated by a mechanically weak, localized shear zone, and that the shear zone persists a considerable distance down-dip from the thrust zone earthquakes.

5. Conclusions

We present a rare example of a thermal model tied to a subduction zone with a geometry constrained independently of seismicity. The results confirm that dehydration reactions can explain the changes in seismic velocities seen within subducting crust. Seismicity within the WBZ lies along a narrow band of p,T conditions, showing a positive slope of 0.1 K/MPa for most consistent models. This geometry is strongly suggestive of a single reaction or step in a sequence of dehydration reactions, which increases pore-fluid pressure in the manner predicted for dehydration embrittlement. Such a pattern has not been seen in the small number of well-instrumented subduction zones, although the small thickness of normal oceanic crust makes such a pattern hard to see elsewhere. Also, the strong effects of layering within normal oceanic crust may dominate the evolution of dehydration and pore pressure, for example by isolating earthquakes near permeability barriers. Finally, simple flow models cannot reproduce the cold viscous nose observed in several subduction zones, a region of low temperatures (usually inferred from seismic attenuation) in the mantle overlying the slabs less than 80 km deep. To reproduce the observed geometry requires that this region be mechanically isolated from the rest of the wedge, perhaps by a localized shear zone extending down-dip from the seismogenic thrust to 80 km depth.

Acknowledgements

We thank B. Hacker and D. Kerrick for discussions, constructive comments from two anonymous reviewers and Associate Editor R. van der Hilst, and the IRIS-PASSCAL Instrument Center for providing field support. This work was supported by the NSF grants EAR 9996451 and 0215577 to Boston University, and EAR 0215534 to the University of Michigan.

References

[1] S.M. Peacock, Thermal structure and metamorphic evolution of subducting slabs, in: J.M. Eiler (Ed.), Inside the Subduction Factory, Geophys. Monogr., vol. 138, AGU, Washington, 2003, pp. 7–22.

[2] B.R. Hacker, S.M. Peacock, G.A. Abers, S.D. Holloway, Subduction factory: 2. Are intermediate-depth earthquakes in subducting slabs linked to metamorphic dehydration reactions?, J. Geophys. Res. 108 (2003) 2030, doi:10.1029/2001JB001129.
[3] P.E. van Keken, B. Kiefer, S.M. Peacock, High-resolution models of subduction zones: implications for mineral dehydration reactions and the transport of water into the deep mantle, Geochem. Geophys. Geosys. 3 (2002) (22-10-2002).
[4] P.B. Kelemen, J.L. Rilling, E.M. Parmentier, L. Mehl, B.R. Hacker, Thermal structure due to solid-state flow in the mantle wedge beneath arcs, in: J.M. Eiler (Ed.), Inside the Subduction Factory, Geophys. Monogr., vol. 138, AGU, Washington, 2003, pp. 293–311.
[5] D. Zhao, T. Matsuzawa, A. Hasegawa, Morphology of the subducting slab boundary in the northeastern Japan arc, Phys. Earth Planet. Inter. 102 (1997) 89–104.
[6] M.G. Bostock, R.D. Hyndman, S. Rondenay, S.M. Peacock, An inverted continental Moho and serpentinization of the forearc mantle, Nature 417 (2002) 536–538.
[7] X. Yuan, S.V. Sobolev, R. Kind, O. Oncken, G. Bock, G. Asch, B. Schurr, F. Graeber, A. Rudloff, W. Hanka, K. Wylegalla, R. Tibi, C. Haberland, A. Rietbrock, P. Giese, P. Wigger, P. Rower, G. Zandt, S. Beck, T. Wallace, M. Pardo, D. Comte, Subduction and collision processes in the central Andes constrained by converted seismic phases, Nature 408 (2000) 958–961.
[8] A. Ferris, G.A. Abers, D.H. Christensen, E. Veenstra, High resolution image of the subducted Pacific plate beneath central Alaska, 50–150 km depth, Earth Planet. Sci. Lett. 214 (2003) 575–588.
[9] M.I. Billen, M. Gurnis, A low viscosity wedge in subduction zones, Earth Planet. Sci. Lett. 193 (2001) 227–236.
[10] D. Arcay, E. Tric, M.P. Doin, Numerical simulations of subduction zones: effect of slab dehydration on the mantle wedge dynamics, Phys. Earth Planet. Inter. 149 (2005) 133–154.
[11] J.C. Stachnik, G.A. Abers, D. Christensen, Seismic attenuation and mantle wedge temperatures in the Alaska subduction zone, J. Geophys. Res. 109 (2004) B10304, doi:10.1029/2004JB003018.
[12] L.A. Preston, K.C. Creager, R.S. Crosson, T.M. Brocher, A.M. Trehu, Intraslab earthquakes: dehydration of the Cascadia slab, Science 302 (2003).
[13] G. Rossi, Measuring the mantle wedge Poisson's ratio and slab depth: central Alaska, M.A. Thesis, Boston University, 2004.
[14] R.L. Saltzer, E. Stutzmann, R.D. van der Hilst, Poisson's ratio in the lower mantle beneath Alaska: evidence for compositional heterogeneity, J. Geophys. Res. 109 (2004) B06301, doi:10.1029/2003JB002712.
[15] S. Karato, H.A. Spetzler, Defect microdynamics in minerals and solid-state mechanisms of seismic wave attenuation and velocity dispersion in the mantle, Rev. Geophys. 28 (1990) 399–421.
[16] I. Jackson, J.D. FitzGerald, U.H. Faul, B.H. Tan, Grain-size-sensitive seismic wave attenuation in polycrystalline olivine, J. Geophys. Res. 107 (2002) 2360, doi:10.1029/2001JB001225.
[17] S. Karato, Mapping water content in the upper mantle, in: J.M. Eiler (Ed.), Inside the Subduction Factory, Geophys. Monogr., vol. 138, Am. Geophys. Union, Washington, 2003, pp. 135–152.
[18] T.T. Gribb, R.F. Cooper, The effect of an equilibrated melt phase on the shear creep and attenuation behavior of polycrystalline olivine, Geophys. Res. Lett. 27 (2000) 2341–2344.
[19] R.D. Hyndman, S.M. Peacock, Serpentinization of the forearc mantle, Earth Planet. Sci. Lett. 212 (2003) 417–432.
[20] C. Kincaid, I.S. Sacks, Thermal and dynamical evolution of the upper mantle in subduction zones, J. Geophys. Res. 102 (1997) 12295–12315.
[21] B. Schurr, G. Asch, A. Rietbrock, R. Trumbull, C. Haberland, Complex patterns of fluid and melt transport in the central Andean subduction zone revealed by attenuation tomography, Earth Planet. Sci. Lett. 215 (2003) 105–119.
[22] Y. Furukawa, S. Uyeda, Thermal state under the Tohoku arc with consideration of crust heat generation, Tectonophysics 164 (1989) 175–187.
[23] R.D. Hyndman, K. Wang, The rupture zone of Cascadia great earthquakes from current deformation and the thermal regime, J. Geophys. Res. 100 (1995) 22133–22154.
[24] M. Springer, A. Forster, Heat-flow density across the central Andean subduction zone, Tectonophysics 291 (1998) 123–139.
[25] R. Von Herzen, C. Ruppel, P. Molnar, M. Nettles, S. Nagihara, G. Ekstrom, A constraint on the shear stress at the Pacific–Australia plate boundary from heat flow and seismicity at the Kermadec forearc, J. Geophys. Res. 106 (2001) 6817–6833.
[26] S.M. Peacock, K. Wang, Seismic consequences of warm versus cool subduction metamorphism: examples from southwest and northeast Japan, Nature 286 (1999) 937–939.
[27] T.M. Brocher, G.S. Fuis, M.A. Fisher, G. Plafker, M.J. Moses, J.J. Taber, N.I. Christensen, Mapping the megathrust beneath the northern Gulf of Alaska using wide-angle seismic data, J. Geophys. Res. 99 (1994) 11663–11685.
[28] C. DeMets, R.G. Gordon, D.F. Argus, S. Stein, Effect of recent revisions to the geomagnetic reversal time-scale to estimates of current plate motions, Geophys. Res. Lett. 21 (1994) 2191–2194.
[29] T. Atwater, Plate tectonic history of the northeast Pacific and western North America, in: E.L. Winterer, D.M. Hussong, R.W. Decker (Eds.), The Eastern Pacific Ocean and Hawaii, The Geology of North America N, Geological Society of America, Boulder, Colorado, 1989, pp. 21–72.
[30] B.R. Hacker, G.A. Abers, S.M. Peacock, Subduction factory: 1. Theoretical mineralogy, density, seismic wavespeeds, and H_2O content, J. Geophys. Res. 108 (2003) 2029, doi:10.1029/2001JB001127.
[31] M.W. Schmidt, S. Poli, Experimentally based water budgets for dehydrating slabs and consequences for arc magma generation, Earth Planet. Sci. Lett. 163 (1998) 361–379.
[32] J.A.D. Connolly, D.M. Kerrick, Metamorphic controls on seismic velocity of subducted oceanic crust at 100–250 km depth, Earth Planet. Sci. Lett. 204 (2002) 61–74.
[33] A.R. Pawley, J.R. Holloway, Water sources for subduction zone volcanism: new experimental constraints, Science 260 (1993) 664–667.
[34] S. Karato, P. Wu, Rheology of the upper mantle—a synthesis, Science 260 (1993) 771–778.
[35] M.A. Eberle, O. Grasset, C. Sotin, A numerical study of the interaction between the mantle wedge, subducting slab, and overriding plate, Phys. Earth Planet. Inter. 134 (2002) 191–202.
[36] G.A. Abers, Hydrated subducted crust at 100–250 km depth, Earth Planet. Sci. Lett. 176 (2000) 323–330.
[37] M.-A. Gutscher, S.M. Peacock, Thermal models of flat subduction and the rupture zone of great subduction earthquakes, J. Geophys. Res. 108 (2003) 2009, doi:10.1029/2001JB000787.
[38] D.M. Kerrick, J.A.D. Connolly, Metamorphic devolatilization of subducted oceanic metabasalts: implications for seismicity, arc magmatism and volatile recycling, Earth Planet. Sci. Lett. 189 (2001) 19–29.

[39] E.F. Baxter, Natural constraints on metamorphic reaction rates, in: D. Vance, W. Müller, I.M. Villa (Eds.), Geochronology: Linking the Isotopic Record with Petrology and Textures, Spec. Pub., vol. 220, Geol. Soc., London, 2003, pp. 183–202 spec. pub. 220.
[40] T.-F. Wong, S.C. Ko, D.L. Olgaard, Generation and maintenance of pore pressure excess in a dehydrating system: 2. Theoretical analysis, J. Geophys. Res. 102 (1997) 841–852.
[41] H. Jung, H.W. Green, L.F. Dobrzhinetskaya, Intermediate-depth earthquake faulting by dehydration embrittlement with negative volume change, Nature 428 (2004) 545–549.
[42] B.W. Tichelaar, L.J. Ruff, Depth of seismic coupling along subduction zones, J. Geophy. Res. 98 (1993) 2017–2037.
[43] C.H. Scholz, Earthquakes and friction laws, Nature 391 (1998) 37–42.
[44] H. Dragert, K. Wang, T.S. James, A silent slip event on the deeper Cascadia subduction interface, Science 292 (2001) 1525–1528.
[45] T.I. Melbourne, W.M. Szeliga, M.M. Miller, V.M. Santillan, Extent and duration of the 2003 Cascadia slow earthquake, Geophys. Res. Lett. 32 (2005) L04301, doi:10.1029/2004GL021790.
[46] S.C. Cohen, J.T. Freymueller, Crustal uplift in the south central Alaska subduction zone: new analysis and interpretation of tide gauge observations, J. Geophys. Res. 106 (2001) 11259–11270.
[47] C.H. Scholz, The Mechanics of Earthquakes and Faulting, Cambridge University Press, Cambridge, 1990. 439 pp.
[48] T. Takanami, S. Sacks, A. Hasegawa, Attenuation structure beneath the volcanic front in northeastern Japan from broad-band seismograms, Phys. Earth Planet. Inter. 121 (2000) 339–357.
[49] E.A. Kneller, P.E. van Keken, S. Karato, J. Park, B-type fabric in the mantle wedge: insights from high-resolution non-Newtonian subduction zone models, Earth Planet. Sci. Lett. 237 (2005) 781–797.
[50] J.A. Conder, A case for hot slab surface temperatures in numerical viscous flow models of subduction zones with an improved fault zone parameterization, Phys. Earth Planet. Inter. 149 (2005).
[51] J.T. Freymueller, S.C. Cohen, H.J. Fletcher, Spatial variations in present-day deformation, Kenai Peninsula, Alaska, and their implications, J. Geophys. Res. 105 (2000) 8079–8101.
[52] T.R. Bruns, Model for the origin of the Yakutat block, an accreting terrane in the northern Gulf of Alaska, Geology 11 (1983) 718–721.